Quantifying Tip-Sample Interactions in Vacuum Using Cantilever-Based Sensors: An Analysis

Omur E. Dagdeviren,[1] Chao Zhou,[1] Eric I. Altman,[2] and Udo D. Schwarz[1,2,*]

[1]*Department of Mechanical Engineering and Materials Science, Yale University, New Haven, Connecticut 06520, USA*

[2]*Department of Chemical and Environmental Engineering, Yale University, New Haven, Connecticut 06520, USA*

(Received 24 November 2017; revised manuscript received 22 February 2018; published 26 April 2018)

Atomic force microscopy is an analytical characterization method that is able to image a sample's surface topography at high resolution while simultaneously probing a variety of different sample properties. Such properties include tip-sample interactions, the local measurement of which has gained much popularity in recent years. To this end, either the oscillation frequency or the oscillation amplitude and phase of the vibrating force-sensing cantilever are recorded as a function of tip-sample distance and subsequently converted into quantitative values for the force or interaction potential. Here, we theoretically and experimentally show that the force law obtained from such data acquired under vacuum conditions using the most commonly applied methods may deviate more than previously assumed from the actual interaction when the oscillation amplitude of the probe is of the order of the decay length of the force near the surface, which may result in a non-negligible error if correct absolute values are of importance. Caused by approximations made in the development of the mathematical reconstruction procedures, the related inaccuracies can be effectively suppressed by using oscillation amplitudes sufficiently larger than the decay length. To facilitate efficient data acquisition, we propose a technique that includes modulating the drive amplitude at a constant height from the surface while monitoring the oscillation amplitude and phase. Ultimately, such an amplitude-sweep-based force spectroscopy enables shorter data acquisition times and increased accuracy for quantitative chemical characterization compared to standard approaches that vary the tip-sample distance. An additional advantage is that since no feedback loop is active while executing the amplitude sweep, the force can be consistently recovered deep into the repulsive regime.

DOI: 10.1103/PhysRevApplied.9.044040

I. INTRODUCTION

With the advent of scanned probe methods, the mapping of interactions between surfaces and a sharp tip featuring the ability to be positioned accurately in the surface's vicinity has become possible [1]. Among the plethora of interactions that are gauged using scanned-probe-based setups, one of the most popular choices, is to explore forces. Initial realizations of the related atomic force microscope [2] relied on measuring the deflection of a soft cantilever that carried a local probe in the form of a sharp tip at its end. With knowledge of the cantilever's spring constant, forces can be recovered while the degree of locality is determined by the dimensions of the tip's apex, and, after contact is established, the size of the tip-sample contact area. Soft cantilevers, however, hamper the ability to position the probe precisely within the immediate three-dimensional (3D) space above the sample's surface due to the so-called "jump-in," which refers to a sudden instability of the tip's position that occurs at the exact distance where the gradient of the attractive surface forces becomes larger than the cantilever's spring constant [3,4]. To avoid the related issues in controlling the tip's position near the surface, for vacuum applications in particular, it has become customary to utilize cantilevers that feature spring constants much higher than the largest force gradient experienced during the approach [5]. While this eliminates jump-ins and, hence, regains an ability to probe the entire 3D space above the surface, it also renders direct force quantification using Hooke's law, which is impracticable, as the high spring constants reduce the cantilever deflections to values that are too small to resolve with sufficient accuracy using current position-sensitive sensors.

As a workaround, "dynamic" operational schemes have been introduced for atomic force microscopy (AFM), where a disturbance of the otherwise harmonic oscillation of the cantilever that is driven at or near its resonance frequency is used to assess the tip-sample distance [6,7]. Among the different possible approaches, two methods are most widespread: the amplitude-modulation (AM) technique, where the change of the oscillation amplitude A and/or the phase

*Corresponding author.
udo.schwarz@yale.edu

difference between oscillation and excitation ϕ while driving with a constant excitation signal are evaluated [8,9], or the frequency-modulation (FM) technique, which tracks the change of the resonance frequency Δf under the influence of the attractive (or repulsive) surface forces while keeping the oscillation amplitude stable [10]. While FM AFM has dominated atomic resolution imaging, in particular, in ultra-high-vacuum conditions [7], AM AFM has its most widespread use in ambient conditions and liquids.

Force spectroscopy experiments are performed to quantify the tip-sample interaction potential as a function of distance (and, by calculating its derivative, ultimately the force) with up to picometer precision laterally with respect to the tip's position relative to the location of the surface atoms, often with the intent to explore the surface's chemical or electronic properties [11–13]. In addition, force spectroscopy experiments are carried out to understand the observed contrast in AFM images [14–17]. Initially, due to the lack of appropriate mathematical models, recovering the quantitative values from the measured signals was conducted indirectly: The recorded signals were compared with either the frequency shifts or oscillation amplitudes or phases calculated numerically when assuming specific model interaction laws. The specifics of the interactions were iteratively adjusted until agreement with the measured data was reached [18–21]. Only after appropriate theoretical tools were developed around the turn of the millennium, was it possible to obtain tip-sample interaction potentials and forces directly from the measured signals [22–30].

In this article, we show that the force laws calculated using the recovery methods most commonly applied under vacuum conditions differ more than previously described from the actual interaction laws when oscillation amplitudes A are used that are comparable to the decay length l of the force. These discrepancies arise because the method uses assumptions that show weaknesses, particularly at $A \approx l$. As a result, the effect of the related disturbances can be minimized by the use of oscillation amplitudes that are either much smaller or much larger than l. Our analysis suggests that under realistic conditions, large oscillation amplitudes are the better choice, while amplitudes comparable to l may still be preferable for imaging. For practical applications, amplitude-sweep-based spectroscopy experiments, which are conducted by tuning the drive amplitude at a constant height from the sample, are suggested as an effective method to recover both the tip-sample force and potential efficiently and accurately deep into the repulsive regime.

II. METHODS

A. Computational methods employed in the theoretical analysis

Following a commonly used approach for dynamic AFM simulations, we solve the equation of motion of a damped harmonic oscillator with external excitation and nonlinear tip-sample interaction force [18,31–33],

$$m\ddot{z}(t) + \frac{2\pi f_0 m}{Q}\dot{z}(t) + c_z[z(t) - d] = a_d c_z \cos(2\pi f_d t) + F_{\mathrm{TS}}[z(t), \dot{z}(t)], \tag{1}$$

where $z(t)$ is the position of the tip as a function of time t (with $z = d$ denoting the distance of the tip relative to the sample when the cantilever is undeflected); m, f_0, Q, and c_z are the effective mass, the first eigenfrequency, the quality factor, and the spring constant of the oscillator, respectively. In this equation, the terms on the left reflect the standard terms for a damped harmonic oscillator, while the first term on the right represents the external excitation of the oscillator with excitation amplitude a_d and excitation frequency f_d. The second term on the right side finally symbolizes the nonlinear tip-sample interaction force F_{TS}, which may depend both on the tip's time-dependent position z as well as its instantaneous velocity $\dot{z}$. Neglecting a possible velocity dependence, we choose F_{TS} in agreement with the previous literature [32,33] as a combination of a van der Waals–type sphere-over-flat interaction [34] for the attractive regime ($z \geq z_0$) and a contact force ($z < z_0$) that follows Maugis's approximation to the Derjaguin-Muller-Toporov model [35–37], which is often referred to as the Hertz-plus-offset model [38]:

$$F_{\mathrm{TS}}(z) = \begin{cases} -\frac{A_H R}{6z^2} & \text{for } z \geq z_0, \\ \frac{4}{3}E^*\sqrt{R}(z_0 - z)^{3/2} - \frac{A_H R}{6z_0^2} & \text{for } z < z_0, \end{cases} \tag{2}$$

where $A_H = 0.2$ aJ is the Hamaker constant, $R = 10$ nm is the radius of the tip's apex, $z_0 = 0.3$ nm is the distance at which the contact is established, and $E^* = [(1-\nu_t^2)/E_t + (1-\nu_s^2)/E_s]^{-1}$ is the combined elastic modulus of the tip and sample (with $E_t = 130$ GPa as the Young's modulus of the tip, $E_s = 1$ GPa as the Young's modulus of the sample, and $\nu_t = \nu_s = 0.3$ as the Poisson ratios of the tip and sample, respectively). To describe the oscillator, we choose $c_z = 2000$ kN and $f_d = f_0 = 22\,000$ Hz; these values reflect the typical parameters for a tuning fork glued on a holder in qPlus configuration, which currently represents the most common oscillator choice for high-resolution vacuum-based AFM.

Equation (1) is then solved by employing two different techniques. First, we numerically compute its solution with MATLAB using MATLAB's ode45 function ("E. O. M." solution; for details, see the Supplemental Material [39]). Second, we apply a previously derived analytical solution for the tip-sample motion, which is, however, defined for conservative tip-sample interactions only [33]. For control purposes, we also extend Eq. (2) by adding a dissipative component following a model introduced in Refs. [41,42],

$$F_{\mathrm{diss}} = F_0 \times e^{-[2z(t)]}\dot{z}(t), \tag{3}$$

where $F_0 = 10^{-7}$ Ns/m, and we subsequently solve the resulting differential equation numerically to investigate

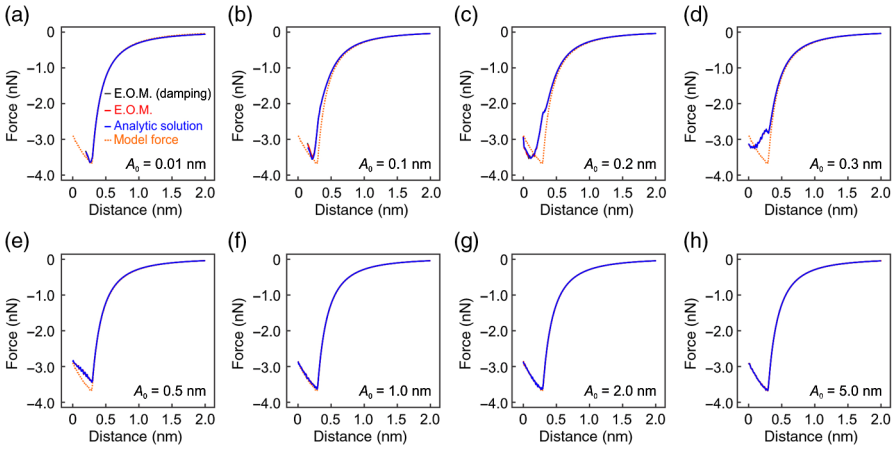

FIG. 1. Comparison between the original model force $F_{\mathrm{TS}}(z)$ Eq. (2) (orange line) and the tip-sample interaction force reconstructed from Eq. (4) using sets of $A(D, A_0)$ and $\phi(D, A_0)$ calculated with the approaches described in Sec. II A for eight different free-oscillation amplitudes A_0. The results show that the different solution methods for Eq. (1) give practically identical results: The black, red, and blue curves always lie right on top of each other so that only the blue curve is visible even though all three curves are plotted in each panel (a–h). The reconstructed force (orange curve), however, deviates noticeably from the actual force for oscillation amplitudes between 0.1 and 0.5 nm.

the effect of a nonconservative tip-sample interaction. The results obtained from this approach are labeled in Figs. 1 and 2 as "E. O. M. (damping)." For all three cases, we determine the oscillation amplitude A and phase ϕ as a function of $z(t)$. Finally, Eq. (4) details the numerical integration method we use for reconstructing the tip-sample interaction potential U_{TS} from data obtained with AM-type force spectroscopy [30,32,43]:

$$U_{\mathrm{TS}}(D) = 2c_z \int_D^\infty \frac{1}{2}\left[\frac{a_d}{A}\cos\phi + \frac{f_0^2 - f_d^2}{f_0^2}\right] \times \left[(z-D) + \sqrt{\frac{A}{16\pi}}\sqrt{z-D} + \frac{A^{3/2}}{\sqrt{2(z-D)}}\right] dz. \tag{4}$$

Note that U_{TS} is given as a function of nearest tip-sample distance D, which distinguishes itself from the distance d the tip has to the surface when the cantilever is undeflected by $D = d - A$. For comparison with FM-type force spectroscopy, we follow the approach introduced by Sader and Jarvis, which represents the most widely used reconstruction protocol for this case [24]. It results in the following equation:

$$U_{\mathrm{TS}}(D) = 2c_z \int_D^\infty \frac{f_0 - f_{\mathrm{res}}}{f_0}\left[(z-D) + \sqrt{\frac{A}{16\pi}}\sqrt{z-D} + \frac{A^{3/2}}{\sqrt{2(z-D)}}\right] dz, \tag{5}$$

where $f_{\mathrm{res}}(D)$ represents the cantilever's distance-dependent resonance frequency (i.e., $\Delta f = f_0 - f_{\mathrm{res}}$). From the similarity of Eqs. (4) and (5), we already see that the same underlying assumptions apply in their derivations, which we discuss later in more detail. With the knowledge of $U_{\mathrm{TS}}(D)$, the tip-sample force F_{TS} as a function of D can easily be recovered for both cases by calculating its negative gradient [$F_{\mathrm{TS}}(D) = -\partial U_{\mathrm{TS}}/\partial D$].

B. Experimental methods

All experiments are carried out under ultrahigh-vacuum conditions at a base pressure of 2×10^{-11} mbar and a temperature of 4 K using a homebuilt microscope, details of which can be found elsewhere [44]. As probe tips,

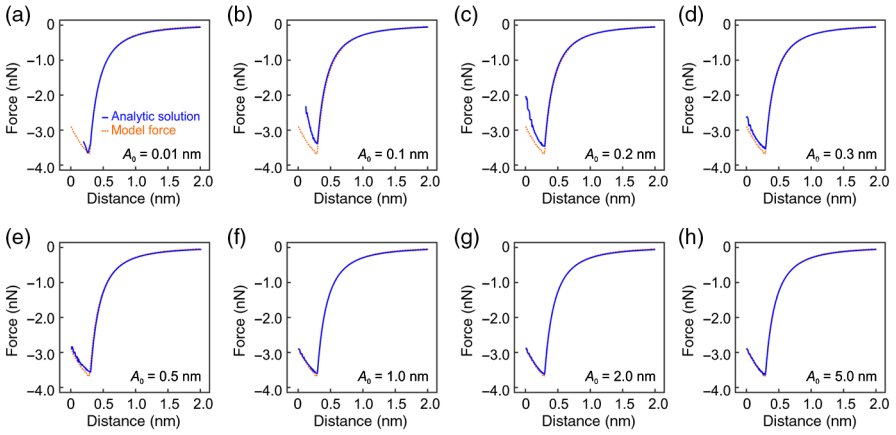

FIG. 2. Analysis of the accuracy of force reconstruction using FM-based spectroscopy. To this end, the blue curve shows $F_{\mathrm{TS}}(D, A_0)$ recovered with Sader and Jarvis's method Eq. (5) from $\Delta f(D, A_0)$ values calculated using the analytical solution to Eq. (1) discussed in Sec. II A, while the orange curve represents the original model force for comparison (a–h). As in Fig. 1, noticeable discrepancies exist for oscillation amplitudes A_0 in the range of 0.1–0.5 nm.

mechanically cut Pt/Ir wires attached to the end of tuning forks arranged in qPlus configuration [45] following an optimized assembly process [46,47] are used. For data acquisition, the microscope is operated using the so-called tuned-oscillator atomic force microscopy (TO AFM) mode [31], which in its essence is a variant of the AM control scheme. However, while conventional AM AFM experiments cannot be conducted under vacuum conditions due to mechanical instabilities and long settling times [10,31], the purposeful tuning of the system's effective quality factor Q_{eff} and a complementary choice of the oscillation amplitude A in TO AFM eliminates mechanical instabilities while drastically reducing settling times. Fine-tuning Q_{eff} and A even allows us to maximize the amplitude drop experienced within the strongly attractive force regime to optimize the imaging conditions [31].

As a prototypical model surface, we use a Pt(111) single crystal, which is cleaned by repetitive sputtering (20 min at 1×10^{-6} mbar Ar background with 1-kV energy) and annealing (1000 K for 20 min) cycles. The topography of an area representative for all locations where the spectroscopy experiments are performed is shown in the Supplemental Material, Fig. S1 [39].

III. RESULTS AND DISCUSSION

A. Force spectroscopy with distance sweep

Thus far, force spectroscopy is overwhelmingly performed by moving the cantilever base relative to the sample surface while measuring the response of the cantilever to the change in the tip-sample interaction potential that the tip experiences as a consequence. Here, we refer to this general approach as the "distance sweep." To start our analysis, we focus first on assessing the accuracy of AM-based force spectroscopy for a tuning fork with tuned oscillation ($Q = 300$) [31]. To this end, we calculate both the oscillation amplitude A and phase ϕ as a function of the nearest tip-sample distance D as described in Sec. II A for eight different free-oscillation amplitudes A_0 and subsequently reconstruct the force by applying Eq. (4) followed by gradient formation. By comparing the results with the original model force Eq. (2), the deviations due to deficiencies in the mathematical procedures can be revealed. From the respective Fig. 1, we extract the following two observations:

(i) The numerical solution of the equation of motion with and without the dissipative term and analytical solution of Eq. (1) match for all calculated free-oscillation amplitudes A_0, which run from 0.01 to 5.0 nm. This not only indicates that for the dissipative force law in Eq. (3) and the range of oscillation amplitudes A_0 investigated, the effect of dissipation is negligible, but also that the analytical solution provides, despite approximations used in its derivation, an accurate and efficient pathway to calculate A and ϕ. Therefore, in the following, we exclusively use these analytical equations to obtain the values of either A/ϕ or Δf to minimize computation time.

(ii) While the agreement between the reconstructed force and model force is high for free-oscillation amplitudes of 1 nm or larger as well as for the smallest amplitude included (0.01 nm), the intermediate values for A_0 show notable deviations once the tip comes close to the surface (distances below approximately 0.6 nm). These deviations manifest both in the *position* and *depth* of the force minimum as well as in marked differences in the *slope* of the force curve near its minimum.

In a next step, we repeat the same procedure for FM-based force spectroscopy assuming a force sensor with a quality factor of $Q = 10\,000$ but otherwise exhibiting our standard values for c_z and f_0 (see Sec. II A). To recover the tip-sample force from those data, we then use Eq. (5) as discussed earlier. While this shows slightly better agreement for oscillation amplitudes between 0.1 and 0.5 nm than in Fig. 1, in particular with respect to the location of the force minimum, it nevertheless exhibits the same trend: good agreement for $A_0 = 1$ nm and larger as well as for $A_0 = 0.01$ nm but noticeable inaccuracy in between.

Summarizing the findings of Figs. 1 and 2, we see that both AM- and FM-based force spectroscopy reproduces the original tip-sample model force well for free-oscillation amplitudes A_0 that are either much larger or much smaller than the decay length l of the attractive section of the force. Thereby, we define l as the distance where the force has diminished to $1/e$ (i.e., about 37%) of its maximum value, which is roughly 0.22 nm for the model force Eq. (2). For $A_0 \approx l$, however, reconstruction yields a systematic underestimation of the interaction strengths during the exact quantitative chemical characterization of specific lattice sites. This underestimation is particularly worth noting because setting $A_0 \approx l$ otherwise results in favorable signal-to-noise values [5], which makes it a popular choice for imaging (e.g., Refs. [5,12,13]). To improve accuracy, our numerical analyses suggest that using oscillation amplitudes sufficiently larger than l is the best way forward since the alternative option $A_0 \ll l$ is likely to produce in comparison inferior signal-to-noise ratios due to the difficulty in precisely measuring small oscillations in realistic experimental setups such as tuning forks. For large A_0, our results show that the reconstructed tip-sample interaction force laws converge with the model force for free-oscillation amplitudes larger than 1 nm.

Ultimately, the behavior described above can be tracked down to the influence of the nonlinear nature of the tip-sample interaction, which poses a variety of challenges for the correct recovery of the potential and assumptions that have to be made. First, we recognize that both Eqs. (4) and (5) are simplifying the math involved by essentially representing a linear combination of two approximations: For $A_0 \ll l$, it presumes that the force changes linearly with

the distance ("gradient approximation"; see, e.g., Refs. [10,19,48]), and for $A_0 \gg l$, it uses a solution obtained by perturbation theory [19,25,26,48–51]. Both approximations are shown to work very well in their respective limits. To describe the behavior in the transition regime (i.e., $A_0 \approx l$), Sader and Jarvis [24] introduced an additional interpolation term that was designed to be mathematically simple while still producing acceptable results, which, due to its success, is also used for deriving Eq. (4) [the $(\sqrt{A/D}\sqrt{z-D})$ term]. In their analysis, Sader and Jarvis quantify the maximum discrepancy from the accurate value with approximately 5% for the specific model force chosen in their paper to occur at $A_0/z_0 \approx 0.3$, where z_0 represents again the location of the force minimum. With this reconstruction $z_0 = 0.3$ nm as in Eq. (2), this predicts that the most deviation should occur for $A_0 \approx 0.1$ nm, which agrees well with the results from Fig. 2. Similarly, Katan *et al.* [43] find the same upper limit of 5% for AM-based spectroscopy when operated with comparable quality factors ($Q = 400$ in their analysis).

Upon closer scrutiny, however, we see that the maximum error found in Fig. 2(b) is approximately 8%, so significantly larger than the 5% both studies report. There could be a variety of reasons, such as the fact that the force law Eq. (2) that we are using differs somewhat from their model force. To check, we use the same force model as in Eq. (2) but divide it by 4 to simulate an interaction of lesser strength. When calculating the maximum deviation for $A_0 = 0.1$ nm for this weaker potential in FM mode, we see that the error drops to about 6.1%, thereby indicating that interactions with larger absolute strength are indeed expected to produce more discrepancies.

While the interpolation inaccuracy discussed above may be the most significant single reason for the discrepancies, we nevertheless expect that other sources of uncertainty have an influence as well. This discrepancy is particularly evident for AM operation because both FM and AM use the same interpolation function, but FM seems to result in somewhat higher accuracy around $A_0 \approx l$. A possible contributor to this distinction may be that for FM, only the relative motion of the resonance curve's highest point (i.e., its actual resonance frequency f_{res}), which shifts under the influence of the surface potential, is tracked. AM operation, however, is locked onto a fixed driving frequency f_d, which is why the shape of the resonance curve may start to play a role. Essentially, its original perfect Lorentzian shape will deform under the influence of an attractive potential in a way that even though TO AFM avoids bifurcations, the shoulder of the resonance curve that includes frequencies $f > f_{\mathrm{res}}$ ("high-frequency shoulder") will be enhanced and the low-frequency shoulder depressed compared to an undisturbed Lorentzian-shaped resonance peak centered at f_{res} as long as the tip-sample interaction is overall attractive [9,33]. If one then sets $f_d = f_0$, where f_0 is again the system's first eigenfrequency, $f_0 > f_{\mathrm{res}}$ as soon as the tip starts to feel the surface; thus, the amplitudes measured upon approach will decay with a lesser slope than if the resonance curve were to be purely Lorentzian. With the relative deviation increasing for decreasing A_0, this effect induces little error for $A_0 \gg l$. In the limit of very small oscillation amplitudes [24,49], however, the gradient approximation term of Eq. (4) contributes most to the potential's total value, which is determined by the *slope* of the amplitude decay with distance $\partial A/\partial D$ rather than the absolute values of A at a particular distance. Since $\partial A/\partial D$ is almost unaffected by curve deformation, no significant deviations are found for $A_0 \ll l$ as well, and this effect again ends up being most significant for the intermediate regime $A_0 \approx l$, as observed.

Before we leave this section, it may be useful to have a look at whether or not some of the inaccuracies pointed out above can be avoided by applying alternative approaches for force reconstruction. For example, Lee and Jhe [27] proposed a method to reconstruct tip-sample interaction forces that is based on using higher-order Bessel functions. Even though their technique can address both conservative and nonconservative forces, it requires multistep integration, which makes the mathematics far more involved than the comparatively easy case of calculating Eqs. (4) or (5). For small oscillation amplitudes, e.g., Bessel functions of the third order are suggested, which necessitate the solution of a seventh-order equation. Another method has been suggested by Shuiqing and Arvind [28], who use Chebyshev polynomials to reconstruct the tip-sample interaction potential. Despite being mathematically complex, the authors themselves found relatively large deviations at small tip-sample separations. Finally, Platz *et al.* [29] introduced a method that is based on the real-time measurement of the cantilever oscillation. To achieve the necessary signal-to-noise ratio, they have to employ large oscillation amplitudes (approximately 20 nm), which are, however, unsuitable for stably operating tuning forks in the attractive regime of the interaction potential under vacuum conditions (note that their method has been developed for potential reconstruction on polymers under ambient conditions). As a result, reconstructing tip-sample potential based on Eqs. (4) or (5) still appears as the most practical course of action.

B. Force spectroscopy with amplitude sweep

As an alternative to distance-sweep-based spectroscopy [or "z-sweep" spectroscopy, indicating that $U_{\mathrm{TS}}(D)$ is recovered by gradually reducing d along the z axis], we propose in this section an approach that keeps the cantilever holder at a fixed distance to the sample surface (i.e., $d = \mathrm{const}$) while ramping up the oscillation amplitude. In the following, we refer to this measurement scheme as "amplitude-sweep" spectroscopy. Similar to the z-sweep spectroscopy of Sec. III A, even though A-sweep spectroscopy can be operated in FM or AM mode, we focus here exclusively on the case of an oscillation-tuned AM

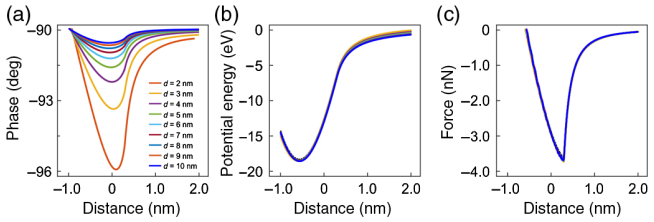

FIG. 3. Numerical calculations for the proposed amplitude-sweep-based spectroscopy technique, where the drive amplitude is ramped up for nine different but otherwise fixed values of d. (a) Phase as a function of the nearest tip-sample distance $D = d - A$. (b) Tip-sample interaction potential $U_{\mathrm{TS}}(D)$ computed by employing Eq. (4). (c) From the data in (b), the tip-sample force F_{TS} is calculated with $F_{\mathrm{TS}}(D) = -\partial U_{\mathrm{TS}}/\partial D$. In panels (b) and (c), we also plot the original model potential and force with dashed black lines. However, since both the tip-sample interaction potential and force are recovered with enhanced accuracy compared to the distance-sweep-based spectroscopy techniques studied in Figs. 1 and 2 and all curves end up essentially lying on top of each other, the dashed black lines are effectively invisible.

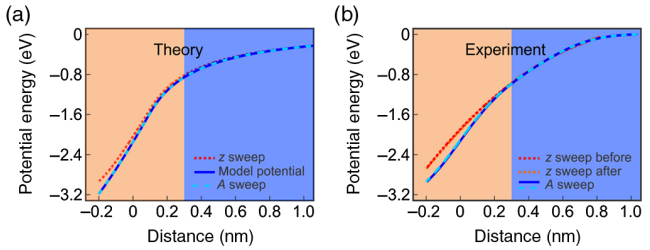

FIG. 4. Comparison of theoretical and experimental results for z- and A-sweep spectroscopy. (a) z-sweep spectroscopy is simulated with a free-oscillation amplitude of 0.22 nm for a tuning fork with tuned oscillation ($c_z = 2000$ N/m, $f_0 = 22\,000$ kHz, $Q = 300$; see Fig. 1), while A-sweep spectroscopy is computed for the same tuning fork but assuming an oscillation amplitude that is ramped up from $A_{\mathrm{min}} = 0$ nm to $A_{\mathrm{max}} = 2.2$ nm with the tip's equilibrium position (i.e., the position of the tip when the cantilever is undeflected) located at a constant distance of $d = 2$ nm. In addition, to adjust the strength of the interaction to the values found in the experiment panel (b), we divide Eq. (2) by 4 before integrating it to obtain the model potential shown with the dark blue solid curve. The results confirm that the interaction potential reconstructed from z-sweep spectroscopy (red dotted line) deviates from this modified model potential, while the data obtained with A-sweep spectroscopy (light blue dashed line) exactly reproduce the original input potential. (b) To assess the validity of the simulations, experiments are conducted for both z- and A-sweep spectroscopy with similar parameters as in (a): $A_0 = 0.22$ nm for z-sweep spectroscopy and $d = 1.07$ nm for A-sweep spectroscopy, ramping A up from $A_{\mathrm{min}} = 0$ nm to $A_{\mathrm{max}} = 1.27$ nm within 2.5 s while collecting 64 data points. Thereby, we conduct z-sweep spectroscopy both before and after recording two curves with A-sweep spectroscopy to verify that the tip does not change during the experiments. During the experiments, the drive frequency of the tuning fork f_d is set to its resonance frequency when the tip is far from the surface, which is found to be $f_0 = 10\,841.2$ Hz, while the quality factor is tuned to $Q_{\mathrm{eff}} = 600$ [31].

approach [31] since, different from FM-based approaches [25], this driving scheme does not require any feedback loop to actively adjust the parameters important for the measurement, e.g., to maintain the amplitude at its set point. Figure 3 shows the summary of a numerical analysis for this approach for nine different distances d that range from 2 to 10 nm; as in Fig. 1, we choose $Q = 300$ as a quality factor. For each of these nine cases, we calculate the phase $\phi(A, d)$ when progressively increasing the oscillation amplitude A from no oscillation (i.e., $A_{\mathrm{min}} = 0$ nm) to $A_{\mathrm{max}} = d + 1$ nm [Fig. 3(a)]. With the values for A and ϕ at hand, we can then recover $U_{\mathrm{TS}}(D)$ from Eq. (4) with $D = d - A$ for any fixed d [Fig. 3(b)] and subsequently F_{TS} by gradient formation [Fig. 3(c)]. Thereby, choosing $A_{\mathrm{max}} = d + 1$ nm sets the minimum distance reached in a sweep to $D = -1$ nm for all cases, which ensures that the potential minimum located at $z \approx -0.57$ nm is within the z range covered. Note that as in Figs. 1 and 2, the location of the zero point on the z axis is determined by the definition of the model force law of Sec. II A, and the surface elastically deforms under the tapping motion of the tip governed by the Hertz-plus-offset term in Eq. (2) in order to reach distances smaller than z_0 (including negative distances). The main findings are (i) positioning the cantilever base at closer distances d produces larger phase shifts; (ii) recovered potentials $U_{\mathrm{TS}}(D)$ are practically identical for all cases, with minor differences at large distances caused by a calibration problem (U_{TS} is set to zero at the largest available tip-sample distance, which is shorter for smaller values of d); (iii) after gradient formation, the model tip-sample force Eq. (2) is accurately recovered in all cases.

Comparing the A- and z-sweep spectroscopy approaches, we find that sweeping the amplitude rather than the distance has a number of advantages. Since the oscillation amplitude increases with decreasing tip-sample separation to more than 1 nm even for the smallest distance d chosen, the experiment is fully within the operational range for which excellent accuracy of the mathematical procedure used to reconstruct the tip-sample interaction potential is found, ultimately leading to the precise reproduction of the theoretical model force found in Fig. 3(c). This situation is further illustrated in Fig. 4, which shows a comparison of theoretical and experimental data for both A- and z-sweep spectroscopy. From Fig. 4(a), the theory shows that performing A-sweep spectroscopy replicates the model potential used for the calculations perfectly, while the z-sweep spectroscopy simulation with a free-oscillation amplitude of 0.22 nm, typical for imaging purposes [5,12,13], results in the discrepancy expected from Fig. 1(c). The complementary experimental results of Fig. 4(b) then show with the example of Pt(111) (see Sec. II B) that A- and z-sweep spectroscopy deviate exactly as predicted, corroborating that our theoretical analysis indeed reproduces the experimental behavior accurately.

One can now argue that the same increase accuracy can easily be achieved with z-sweep spectroscopy as well if one just runs the approach curves with amplitudes larger than 1 nm. Amplitude-sweep-based spectroscopy has, however, further advantages that may make its application beneficial. For example, scanner nonlinearities and piezo creep effects are avoided, which enhances the lateral accuracy of spectroscopy experiments [52]. Also, we note that A-sweep spectroscopy performed in ultrahigh vacuum should be conducted with TO AFM to decrease the cantilever's effective quality factor Q_{eff} to a value that provides the best combination of short settling times ("time constants") $\tau = Q_{\mathrm{eff}}/\pi f_0$ [10] and measurable effect of the surface potential on the phase $\phi(A, d)$ while eliminating mechanical instabilities during the cantilever's approach to the surface [31]. Thanks to the shorter time constants which reflect the time needed to meaningfully acquire an individual data point, faster data acquisition times can be realized that have the prospect to enable 3D imaging during an individual scan [13,52,53]. To achieve this goal, one can, e.g., ramp up the oscillation amplitude at each pixel during a constant-height scan to recover the tip-sample interaction. Alternatively, one can image with a set amplitude of, e.g., 1–2 nm, and record the decay of A [42]. A tuning fork with 22 000-Hz resonance frequency operated at $Q_{\mathrm{eff}} = 300$ features a time constant of around 4 ms, which adds up to approximately 1 min to acquire a single x-z plane with 256×64 pixels or 4.5 h to complete a full 3D set comprising $256 \times 256 \times 64$ data points, which has to be compared with typically 10 times as long acquisition periods for 3D force spectroscopy performed in ultrahigh vacuum [11,13,52,54–56]. Finally, amplitude-sweep spectroscopy experiments with TO AFM are straightforward to control as they are entirely open loop, while FM-based distance-sweep experiments require two feedback loops to be active: one that continuously adjusts the driving frequency to match the cantilever's distant-dependent resonant frequency, a task typically performed by a phase-locked loop [57], and a second loop that maintains a constant oscillation amplitude. As a consequence, probing repulsive forces is straightforward with oscillation-tuned A-sweep spectroscopy but not for FM-based z-sweep spectroscopy, which struggles due to the large tapping-induced perturbation that two interacting feedback loops attempt to address simultaneously.

IV. SUMMARY AND CONCLUSIONS

Thanks to recent advances in three-dimensional imaging, chemical interactions at and near surfaces can be measured locally with picometer, piconewton, and milli-electron volt resolution in space, tip-sample force, and interaction potential. As a consequence, dynamic atomic force microscopy methods have increasingly been used as a quantitative imaging tool to probe local chemistry, an endeavor for which accurate force and potential energy measurements are essential. However, when using oscillation amplitudes of the order of the decay length l of the tip-sample interaction force, the nonlinear nature of the force law is found to introduce a systematic error into the mathematical procedures used to reconstruct the tip-sample force due to a decreased accuracy of some of the approximations made when deriving the procedures. It is possible to decrease the effect of these systematic errors by using oscillation amplitudes sufficiently larger than l. Therefore, although oscillation amplitudes comparable to l should be used to achieve the best signal-to-noise ratio during imaging, choosing the ideal oscillation amplitude for force spectroscopy experiments is an optimization problem between the best signal-to-noise ratio and the accuracy of the obtained quantitative values after force reconstruction. To this end, amplitude-sweep spectroscopy performed at a constant height from the surface promises a pathway toward accurate, faster, and easier force spectroscopy experiments.

ACKNOWLEDGMENTS

We thank Dr. Hendrik Hölscher for fruitful discussions. As this method development directly benefits multiple projects, it is equally supported by the National Science Foundation through Grant No. CHE-1608568 and the Department of Energy through Grant No. DE-SC0016179, which both provide funding for O. E. D. In addition, C. Z.'s participation in the project is enabled by the National Science Foundation Grant No. MRSEC DMR-1119826.

[1] D. A. Bonnell, D. N. Basov, M. Bode, U. Diebold, S. V. Kalinin, V. Madhavan, L. Novotny, M. Salmeron, U. D. Schwarz, and P. S. Weiss, Imaging physical phenomena with local probes: From electrons to photons, Rev. Mod. Phys. **84**, 1343 (2012).

[2] G. Binnig, C. F. Quate, and C. Gerber, Atomic Force Microscope, Phys. Rev. Lett. **56**, 930 (1986).

[3] N. A. Burnham, R. J. Colton, and H. M. Pollock, Interpretation of force curves in force microscopy, Nanotechnology **4**, 64 (1993).

[4] S. Yongho and J. Wonho, Atomic force microscopy and spectroscopy, Rep. Prog. Phys. **71**, 016101 (2008).

[5] F. J. Giessibl, H. Bielefeldt, S. Hembacher, and J. Mannhart, Calculation of the optimal imaging parameters for frequency modulation atomic force microscopy, Appl. Surf. Sci. **140**, 352 (1999).

[6] R. García and R. Pérez, Dynamic atomic force microscopy methods, Surf. Sci. Rep. **47**, 197 (2002).

[7] F. J. Giessibl, Advances in atomic force microscopy, Rev. Mod. Phys. **75**, 949 (2003).

[8] Y. Martin, C. C. Williams, and H. K. Wickramasinghe, Atomic force microscope-force mapping and profiling on a sub 100-Å scale, J. Appl. Phys. **61**, 4723 (1987).

[9] R. Garcia, *Amplitude Modulation Atomic Force Microscopy* (Wiley-VCH, Singapore, 2010).

[10] T. R. Albrecht, P. Grütter, D. Horne, and D. Rugar, Frequency modulation detection using high-Q cantilevers for enhanced force microscope sensitivity, J. Appl. Phys. **69**, 668 (1991).
[11] L. Gross, F. Mohn, N. Moll, P. Liljeroth, and G. Meyer, The chemical structure of a molecule resolved by atomic force microscopy, Science **325**, 1110 (2009).
[12] L. Gross, F. Mohn, P. Liljeroth, J. Repp, F. J. Giessibl, and G. Meyer, Measuring the charge state of an adatom with noncontact atomic force microscopy, Science **324**, 1428 (2009).
[13] B. J. Albers, T. C. Schwendemann, M. Z. Baykara, N. Pilet, M. Liebmann, E. I. Altman, and U. D. Schwarz, Three-dimensional imaging of short-range chemical forces with picometre resolution, Nat. Nanotechnol. **4**, 307 (2009).
[14] M. Ondráček, C. González, and P. Jelínek, Reversal of atomic contrast in scanning probe microscopy on (111) metal surfaces, J. Phys. Condens. Matter **24**, 084003 (2012).
[15] M. Ondráček, P. Pou, V. Rozsíval, C. González, P. Jelínek, and R. Pérez, Forces and Currents in Carbon Nanostructures: Are We Imaging Atoms?, Phys. Rev. Lett. **106**, 176101 (2011).
[16] S. Bartosz, G. Thilo, K. Shigeki, M. Ernst, T. Robert, B. Ján, and Š. Ivan, Interplay of the tip-sample junction stability and image contrast reversal on a Cu(111) surface revealed by the 3D force field, Nanotechnology **23**, 045705 (2012).
[17] O. E. Dagdeviren, J. Götzen, E. I. Altman, and U. D. Schwarz, Exploring site-specific chemical interactions at surfaces: a case study on highly ordered pyrolytic graphite, Nanotechnology **27**, 485708 (2016).
[18] B. Anczykowski, D. Krüger, K. L. Babcock, and H. Fuchs, Basic properties of dynamic force spectroscopy with the scanning force microscope in experiment and simulation, Ultramicroscopy **66**, 251 (1996).
[19] F. J. Giessibl, Forces and frequency shifts in atomic-resolution dynamic-force microscopy, Phys. Rev. B **56**, 16010 (1997).
[20] B. Anczykowski, J. P. Cleveland, D. Krüger, V. Elings, and H. Fuchs, Analysis of the interaction mechanisms in dynamic mode SFM by means of experimental data and computer simulation, Appl. Phys. A **66**, S885 (1998).
[21] B. Gotsmann, B. Anczykowski, C. Seidel, and H. Fuchs, Determination of tip-sample interaction forces from measured dynamic force spectroscopy curves, Appl. Surf. Sci. **140**, 314 (1999).
[22] J. E. Sader and S. P. Jarvis, Coupling of conservative and dissipative forces in frequency-modulation atomic force microscopy, Phys. Rev. B **74**, 195424 (2006).
[23] E. S. John, U. Takayuki, J. H. Michael, F. Alan, N. Yoshikazu, and P. J. Suzanne, Quantitative force measurements using frequency modulation atomic force microscopy—Theoretical foundations, Nanotechnology **16**, S94 (2005).
[24] J. E. Sader and S. P. Jarvis, Accurate formulas for interaction force and energy in frequency modulation force spectroscopy, Appl. Phys. Lett. **84**, 1801 (2004).
[25] H. Hölscher, W. Allers, U. D. Schwarz, A. Schwarz, and R. Wiesendanger, Determination of Tip-Sample Interaction Potentials by Dynamic Force Spectroscopy, Phys. Rev. Lett. **83**, 4780 (1999).
[26] U. Dürig, Relations between interaction force, and frequency shift in large-amplitude dynamic force microscopy, Appl. Phys. Lett. **75**, 433 (1999).
[27] M. Lee and W. Jhe, General Theory of Amplitude-Modulation Atomic Force Microscopy, Phys. Rev. Lett. **97**, 036104 (2006).
[28] H. Shuiqing and R. Arvind, Inverting amplitude and phase to reconstruct tip-sample interaction forces in tapping mode atomic force microscopy, Nanotechnology **19**, 375704 (2008).
[29] D. Platz, D. Forchheimer, E. A. Tholén, and D. B. Haviland, Interaction imaging with amplitude-dependence force spectroscopy, Nat. Commun. **4**, 1360 (2013).
[30] F. P. Amir, M.-J. Daniel, and G. Ricardo, Force reconstruction from tapping mode force microscopy experiments, Nanotechnology **26**, 185706 (2015).
[31] O. E. Dagdeviren, J. Götzen, H. Hölscher, E. I. Altman, and U. D. Schwarz, Robust high-resolution imaging and quantitative force measurement with tuned-oscillator atomic force microscopy, Nanotechnology **27**, 065703 (2016).
[32] H. Hölscher, Theory of phase-modulation atomic force microscopy with constant-oscillation amplitude, J. Appl. Phys. **103**, 064317 (2008).
[33] H. Hölscher and U. D. Schwarz, Theory of amplitude modulation atomic force microscopy with and without Q-control, Int. J. Nonlinear Mech. **42**, 608 (2007).
[34] J. Israelachvili, *Intermolecular and Surface Forces*, 2nd ed. (Academic Press, London, 1991).
[35] U. D. Schwarz, A generalized analytical model for the elastic deformation of an adhesive contact between a sphere and a flat surface, J. Colloid Interface Sci. **261**, 99 (2003).
[36] D. Maugis and B. Gauthier-Manuel, JKR-DMT transition in the presence of a liquid meniscus, J. Adhes. Sci. Technol. **8**, 1311 (1994).
[37] J. A. Greenwood and K. L. Johnson, An alternative to the Maugis model of adhesion between elastic spheres, J. Phys. D **31**, 3279 (1998).
[38] U. D. Schwarz, O. Zwörner, P. Köster, and R. Wiesendanger, Quantitative analysis of the frictional properties of solid materials at low loads. I. Carbon compounds, Phys. Rev. B **56**, 6987 (1997).
[39] See Supplemental Material at http://link.aps.org/supplemental/10.1103/PhysRevApplied.9.044040 for details concerning surface cleanliness and solving the equation of motion, which includes Refs. [6,10,31,33,35–37,40].
[40] C. J. Chen, *Introduction to Scanning Tunneling Microscopy* (Oxford University Press, New York, 1993).
[41] H. Hölscher, B. Gotsmann, and A. Schirmeisen, Dynamic force spectroscopy using the frequency modulation technique with constant excitation, Phys. Rev. B **68**, 153401 (2003).
[42] H. Hölscher, Q-controlled dynamic force spectroscopy, Surf. Sci. **515**, 517 (2002).
[43] A. J. Katan, M. H. van Es, and T. H. Oosterkamp, Quantitative force versus distance measurements in amplitude modulation AFM: A novel force inversion technique, Nanotechnology **20**, 165703 (2009).
[44] B. J. Albers, M. Liebmann, T. C. Schwendemann, M. Z. Baykara, M. Heyde, M. Salmeron, E. I. Altman, and U. D. Schwarz, Combined low-temperature scanning tunneling/atomic force microscope for atomic resolution imaging and

site-specific force spectroscopy, Rev. Sci. Instrum. **79**, 033704 (2008).

[45] F. J. Giessibl, High-speed force sensor for force microscopy and profilometry utilizing a quartz tuning fork, Appl. Phys. Lett. **73**, 3956 (1998).

[46] O. E. Dagdeviren and U. D. Schwarz, Optimizing qPlus sensor assembly for simultaneous scanning tunneling and noncontact atomic force microscopy operation based on finite element method analysis, Beilstein J. Nanotechnol. **8**, 657 (2017).

[47] O. E. Dagdeviren and U. D. Schwarz, Numerical performance analysis of quartz tuning fork-based force sensors, Meas. Sci. Technol. **28**, 015102 (2017).

[48] H. Hölscher, U. D. Schwarz, and R. Wiesendanger, Calculation of the frequency shift in dynamic force microscopy, Appl. Surf. Sci. **140**, 344 (1999).

[49] F. J. Giessibl, A direct method to calculate tip-sample forces from frequency shifts in frequency-modulation atomic force microscopy, Appl. Phys. Lett. **78**, 123 (2001).

[50] H. Hölscher, A. Schwarz, W. Allers, U. D. Schwarz, and R. Wiesendanger, Quantitative analysis of dynamic-force-spectroscopy data on graphite(0001) in the contact and noncontact regimes, Phys. Rev. B **61**, 12678 (2000).

[51] U. D. Schwarz, H. Hölscher, and R. Wiesendanger, Atomic resolution in scanning force microscopy: Concepts, requirements, contrast mechanisms, and image interpretation, Phys. Rev. B **62**, 13089 (2000).

[52] M. Z. Baykara, O. E. Dagdeviren, T. C. Schwendemann, H. Mönig, E. I. Altman, and U. D. Schwarz, Probing three-dimensional surface force fields with atomic resolution: Measurement strategies, limitations, and artifact reduction, Beilstein J. Nanotechnol. **3**, 637 (2012).

[53] M. Z. Baykara, T. C. Schwendemann, E. I. Altman, and U. D. Schwarz, Three-dimensional atomic force microscopy—Taking surface imaging to the next level, Adv. Mater. **22**, 2838 (2010).

[54] M. Ashino, D. Obergfell, M. Haluška, S. Yang, A. N. Khlobystov, S. Roth, and R. Wiesendanger, Atomically resolved mechanical response of individual metallofullerene molecules confined inside carbon nanotubes, Nat. Nanotechnol. **3**, 337 (2008).

[55] D. A. Braun, D. Weiner, B. Such, H. Fuchs, and A. Schirmeisen, Submolecular features of epitaxially grown PTCDA on Cu(111) analyzed by force field spectroscopy, Nanotechnology **20**, 264004 (2009).

[56] S. Fremy, S. Kawai, R. Pawlak, T. Glatzel, A. Baratoff, and E. Meyer, Three-dimensional dynamic force spectroscopy measurements on KBr(001): Atomic deformations at small tip–sample separations, Nanotechnology **23**, 055401 (2012).

[57] C. Loppacher, M. Bammerlin, F. Battiston, M. Guggisberg, D. Müller, H. R. Hidber, R. Lüthi, E. Meyer, and H. J. Güntherodt, Fast digital electronics for application in dynamic force microscopy using high-Q cantilevers, Appl. Phys. A **66**, S215 (1998).